Molecular Vision 2016; 22:536-547 <http://www.molvis.org/molvis/v22/536>
Received 4 July 2015 | Accepted 26 May 2016 | Published 28 May 2016

Stage-specific differentiation of iPSCs toward retinal ganglion cell lineage

Fei Deng,[1] Mengfei Chen,[1] Ying Liu,[1] Huiling Hu,[2] Yunfan Xiong,[1] Chaochao Xu,[1] Yuchun Liu,[1] Kangjun Li,[1] Jing Zhuang,[1] Jian Ge[1]

[1]State Key Laboratory of Ophthalmology, Zhongshan Ophthalmic Center, Sun Yat-sen University, Guangzhou, China; [2]Shengzhen Ophthalmic Center of Jinan University, Shenzhen Eye Hospital, Shenzhen, China

Purpose: As an alternative and desirable approach for regenerative medicine, human induced pluripotent stem cell (hiPSC) technology raises the possibility of developing patient-tailored cell therapies to treat intractable degenerative diseases in the future. This study was undertaken to guide human Tenon's capsule fibroblasts-derived iPSCs (TiPSCs) to differentiate along the retinal ganglion cell (RGC) lineage, aiming at producing appropriate cellular material for RGC regeneration.

Methods: By mimicking RGC genesis, we deliberately administered the whole differentiation process and directed the stage-specific differentiation of human TiPSCs toward an RGC fate via manipulation of the retinal inducers (DKK1+Noggin+Lefty A) alongside master gene (*Atoh7*) sequentially. Throughout this stepwise differentiation process, changes in primitive neuroectodermal, eye field, and RGC marker expression were monitored with quantitative real-time PCR (qRT-PCR), immunocytochemistry, and/or flow cytometry.

Results: Upon retinal differentiation, a large fraction of the cells developed characteristics of retinal progenitor cells (RPCs) in response to simulated environment signaling (DKK1+Noggin+Lefty A), which was selectively recovered with manual isolation approaches and then maintained in the presence of mitogen for multiple passages. Thereafter, overexpression of *ATOH7* further promoted RGC specification in TiPSC-derived RPCs. A subset of transfected cells displayed RGC-specific expression patterns, including Brn3b, iSlet1, calretinin, and Tuj, and approximately 23% of *Brn3b*-positive RGC-like cells were obtained finally.

Conclusions: Our DKK1+Noggin+Lefty A/*Atoh7*-based RGC-induction regime could efficiently direct TiPSCs to differentiate along RGC lineage in a stage-specific manner, which may provide a benefit to develop possible cell therapies to treat retinal degenerative diseases such as glaucoma.

The clinical translation of induced pluripotent stem cell (iPSC) techniques to cell-based regenerative therapies in human degenerative diseases has been made a priority worldwide. Throughout the whole body, the eye is an ideal target for regenerative medicine study, due to the eye's immune privilege attribute and relative ease of accessibility [1]. Recently, the world's first iPSC clinical trial involving macular degeneration was undertaken in Japan [2,3] in an attempt to restore patients' vision by transplanting iPSC-derived RPE (hiPSC-RPE). This has important implications for exploring novel therapeutic strategies for other retinal neurodegenerative diseases, such as glaucoma.

As a type of optic neuropathy, glaucoma is the leading cause of worldwide irreversible blindness, affecting an estimated 67 million people. The primary risk factor associated with glaucoma is an increase in intraocular pressure, which causes RGC loss in a characteristic pattern. Since mature mammalian RGCs do not regenerate after injury [4], it would be of great benefit to design a method to replace degenerative RGCs. Recent innovative three-dimensional (3D) culture studies [5-7] have demonstrated hiPSCs' intrinsic potential to self-form stratified eye cup–like structures, which consist of relevant retinal cell types including RGCs. However, a protracted and continuous culture period is required to gain a small number of RGCs in a mixed cell pool, and the RGC portion gradually disappears as the cultures continue. In this regard, 3D culture does not seem suitable for sufficient RGC derivation to sustain clinical use. In addition, generating multilayered mature retinal tissue may not be required for future cell-therapy strategies that are based on purified retinal specific cells. Thus, selectively guiding iPSCs along RGC lineage differentiation may offer a sufficient quantity of desired donor cells for glaucoma treatment.

Although iPSCs have been shown to display a propensity to produce cells with retinal characteristics [8,9], this limited competence is far from enough to achieve targeted RGC differentiation by iPSCs' multipotency nature [10,11], and much remains to be done to enhance RGC differentiation.

Correspondence to: Jian Ge, State Key Laboratory of Ophthalmology, Zhongshan Ophthalmic Center, Sun Yat-sen University, 54S Xian Lie Road, Guangzhou 510060, China; Phone: 86-20-87331374; FAX: 86-20-87333271; email: gejian@mail.sysu.edu.cn

During retinogenesis, human embryonic stem cells (hESCs) undergo a stepwise and conserved developmental process through primitive eye field (EF) and retinal progenitor cell (RPC) stages toward committed neuronal subtypes [9]. Thus, achieving highly homogeneous RPC differentiation is necessary for subsequent RGC induction. Various exogenous molecules involved in retinal neurogenesis have been used in previous studies to boost RPC generation. Among them, DKK1, Noggin, and Lefty A (the inhibitors of the Wnt, bone morphogenetic protein (BMP), and nodal signaling pathways, respectively [12-16]) are the three retinal-inducing factors used most often in the dish to push iPSCs toward the neuroretinal fate.

During the late histogenesis stage, progenitor cells progressively exit mitosis and sequentially differentiate into one of seven basic retinal cell subtypes. In vertebrate retinas, RGCs are invariably the first neuronal subtype to be established [17]. Coinciding with the onset of retinal neurogenesis, basic helix–loop–helix transcription factor *Ath5* (*Math5* in mice, *lakritz* in zebrafish, *Cath5* in chicks, and *Xath5* in *Xenopus*), ortholog of the Drosophila proneural gene *Atonal*, is one of the first transcription factors to be expressed in RPCs and plays a key role in the establishment of RGC competence and subsequent control of RGC differentiation [18-20]. In developing retinas, null mutation of *Math5* in mice [21,22] and *lakritz* in zebrafish [23] lead to almost complete absence of RGCs, whereas overexpression of *Cath5* in chicks [24] and *Xath5* in *Xenopus* [25,26] exclusively promote RGC production, which strongly suggests the important role of *Ath5* in RGC genesis. Likewise, an in vitro study has also demonstrated the RGC-inducing function of *Math5* in the context of a mouse iPSC line [27]. However, to date, no human iPSC lines have been used to test the validity of directing RGC differentiation genetically. Given the central role of *Ath5* in RGC commitment and the evolutionarily conserved neurogenic process, we propose that overexpression of *ATOH7* (Gene ID 220202, OMIM 609875; a human *Atonal* homolog) in vitro could bias RPCs toward a RGC fate not only from mouse iPSCs as has been reported but also from human iPSCs.

Understanding the developmental requirements of RGCs may definitely play an important role in priming iPSCs toward RGC differentiation in a selective manner. In this study, we used our established human Tenon's capsule fibroblasts-derived iPSCs (TiPSCs) [28] for the specific RGC induction. As Tenon's capsule fibroblasts can be easily obtained during glaucoma surgery, we propose that TiPSCs may serve as a clinically available cell source for RGC regeneration research. Thus, by mimicking the natural developmental process of RGCs, we performed a stepwise induction strategy combined with DKK1+Noggin+Lefty A (DNL) treatment and *Atoh7* overexpression sequentially. Upon retinal differentiation, the TiPSCs initially yielded a highly enriched cell population with an early eye field fate in serum-free medium with the addition of the factor combination. Thereafter, overexpression of *ATOH7* further promoted RGC specification in TiPSC-derived RPCs. Results from this study demonstrate that TiPSCs can efficiently generate RGC-like cells in a stage-specific manner by responding to early and late retinal developmental stimulus respectively. We hope our DKK1+Noggin+Lefty A/*Atoh7*-based RGC-induction regime facilitates the use of hiPSCs in glaucoma treatment.

METHODS

Human TiPSC maintenance culture: The human Tenon's capsule fibroblasts (HTFs)-derived iPSCs (TiPSCs) used in this paper have been established before [28]. Tenon's capsule samples were obtained with written informed consent in adherence with the Declaration of Helsinki and the ARVO statement on human subjects, and with approval from the institutional review board at ZhongShan Ophthalmic Center (ID: 20140311). HTFs were reprogrammed to TiPSCs by retroviral transduction of OCT4, SOX2, C-Myc and KIF4. The resulting TiPSC colonies were maintained on mitomycin C-inactived mouse embryonic fibroblast (MEF) feeder cells in hESC medium as previously described: Dulbecco's Modified Eagle Medium/F12 (DMEM/F12, 1:1; Gibco; Carlsbad, CA) supplemented with 20% knockout serum replacement, 0.1 mM nonessential amino acids, 1 mM L-glutamine, 0.1 mM β-mercaptoethanol, 50 units/ml penicillin, 50 μg/ml streptomycin (all from Gibco), 10 ng/ml basic fibroblast growth factor (bFGF; PeproTech, Rocky Hill, NJ), and 5 μg/ml Plasmocin (InvivoGen, San Diego, CA). The medium was changed daily. For further culture, morphologically identifiable differentiated cells were mechanically removed, and TiPSCs were passaged every 5 to 6 days. All of the cells used in this study were cultured in a 37 °C humidified incubator containing 5% CO_2.

Stepwise induction and expansion of retinal progenitor cells from TiPSCs: To cause TiPSCs to differentiate toward retinal progenitor cell (RPC) fate, previous protocols described for hESC differentiation were adopted in our study with some modifications [9]. Figure 1 shows a schematic diagram of our stepwise differentiation approach. Briefly, the TiPSC colonies were harvested approximately 1 day before normal subculture and placed in six-well ultralow-attachment plates (Corning Costar, Kennebunk, ME) without feeders for free-floating embryoid body (EB) formation in serum-free EB

medium (removal of bFGF from the hESC medium). During the suspension culture, recombinant proteins Dkk1 (Wnt antagonist, 100 ng/ml; R&D Systems, Minneapolis, MN), Lefty A (nodal antagonist, 100 ng/ml; R&D Systems), and Noggin (BMP inhibitor, 100 ng/ml; PeproTech) were added to the EB medium from day 2 to day 6 for differentiation. The medium was changed every 2 days by sedimentation. Six days later, EB aggregates were then replated in a Matrigel-coated (1:3 dilution; BD Biosciences, Bedford, MA) culture dish at a ratio of one well of EBs to one well of a six-well plate and switched to neural differentiation medium (NDM): Neurobasal medium containing serum-free supplement B_{27} (minus vitamin A) and N_2, 0.1 mM nonessential amino acids, 1 mM L-glutamine, and 0.1 mM β-mercaptoethanol (all from Gibco). Recombinant proteins were applied as the EB medium for another 10 days with medium changes every other day. On day 16, the loosely adherent central portions of the neural aggregates were selectively detached and reseeded on Matrigel-coated six-well plates as Passage 0 (neural clump P0) for RPC purification and outgrowth in RPC medium (removing recombinant proteins from NDM, adding 20 ng/ml bFGF/epidermal growth factor [EGF], and 100 ng/ml NGF). After incubating for another 5 to 10 days, the neuroepithelial cells that emerged from the aggregates were then collected and dissociated into single cells with TrypLE (Gibco) treatment, replated at a high density of 1–1.5×10^6 cells/ml in RPC medium+1% Matrigel as Passage 1 (single cell P1), and further propagated at a ratio of 1:3 or 1:4 with TrypLE approximately once a week. Before differentiation, cells may also be frozen at this stage to generate a bank of developmentally similar cell populations.

Generation of retinal ganglion–like cells by overexpression of Atoh7: For subsequent RGC differentiation, RPCs were passaged at a density of 5×10^5 cells/ml on 12-well plates. After 2 to 3 days, porcine cytomegalovirus- green fluorescent protein pCMV-*Atoh7* expression plasmids (constructed in GeneCopoeia, Inc., Rockville, MD) were transfected into RPC cells. Briefly, 3 h before transfection, fresh medium without antibiotics was replaced, and transfection was done with 4 µg plasmid (diluted in neurobasal medium to a concentration of 1 µg/100 µl) and 12 µl X-tremeGENE HP DNA Transfection Reagent (Roche, Basel, Switzerland). The DNA/Reagent mixture (100 µl/well) was added dropwise to RPC cells with the addition of 10 µM DAPT (γ-secretase inhibitor; Calbiochem, San Diego, CA). pCMV-GFP (plasmid 11153; Addgene, Cambridge, MA) expression plasmid was prepared in parallel as a control to monitor infection efficiency. Functional studies were performed 1 week post-transfection.

Quantitative real-time PCR: Total RNA was isolated using TRIzol reagent (Ambion, Austin, TX) and first-strand cDNA was synthesized with SuperScript III Platinum One-Step qRT-PCR Kit (Life, Carlsbad, CA) according to manufacturer's instructions. Quantitative PCR was performed using SYBR Green I (Life) on an ABI 7500 fast system (Life). Reactions were achieved in triplicate, Ct values were calculated using the $2^{-\Delta\Delta C}$t method and the expression of target genes were normalized to ACTB expression. Primer sequences are listed in Table 1.

Immunofluorescence: Cells were immunolabeled as described previously [28]. Briefly, EBs and cell samples were fixed in 4% paraformaldehyde for 10–15 min, permeabilized with 0.1% Triton X-100/PBS (1X; 140 mM NaCl, 10 mM KCl, 8 mM Na_2HPO_4, 2 mM KH_2PO_4, pH 7.4; Thermo Scientific, Rockford, IL) for 10 min, blocked in 4% bovine serum albumin (BSA) for 30 min, and incubated with primary antibodies overnight at 4 °C. The next day, the samples were washed three times with PBS and subsequently incubated with Alexa Fluor 488 or 555 labeled secondary antibody (1:300, Invitrogen) for 30 min at room temperature in the dark. After washing three times with PBS, the samples were counterstained with 4',6-diamidino-2-phenylindole (DAPI, 1 µg/ml; Molecular Probes, Carlsbad, CA). Primary

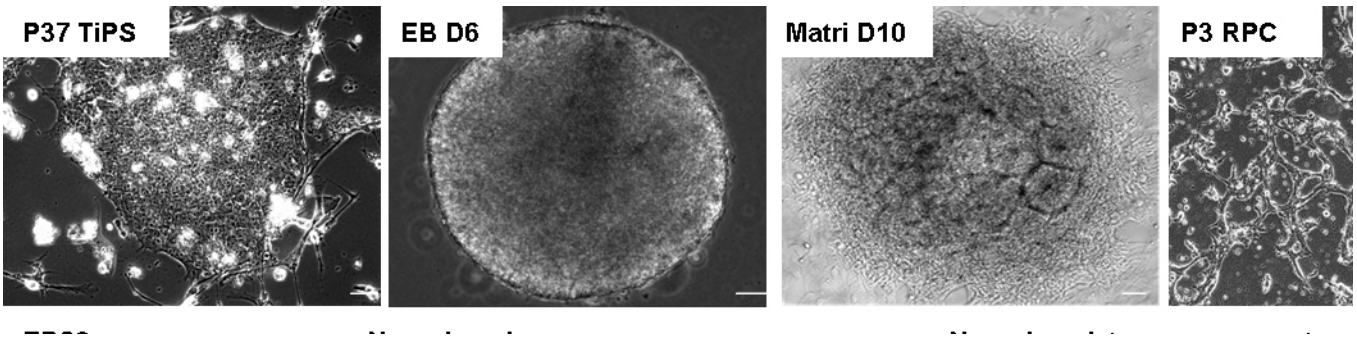

Figure 1. Schematic of the protocol for the generation of RGCs from human Tenon's-derived iPSCs. EB = embryonic body. RPC = retinal progenitor cells. Scale bars = 50 µm.

Table 1. Primer sequences used in real-time PCR.

Gene name	Primer sequence (5′-3′)	Accession number
Oct-4	GGAGGAAGCTGACAACAATGAAA	NM_001285987
(POU5F1)	TACAGAACCACACTCGGACCAC	
NANOG	GCAAGAACTCTCCAACATCCTGA	NM_024865
	CCTTCTGCGTCACACCATTG	
PAX6	GAATGGGCGGAGTTATGATACCTA GAAATGAGTCCTGTTGAAGTGGTG	NM_001258465
SOX2	ACACTCACGCAAAAACCGC AAAGCTCCTACCGTACCACTAGAACT	NM_003106
LHX2	CAACCCTCTGGGTCTTCCCT GTGCTCTGCGTCGTTTTCGT	NM_004789
RAX	GCGTTCGAGAAGTCCCACTAC	NM_013435
	GTCGGTTCTGGAACCACACC	
CHX10 (VSX2)	GCTACTGGGGATGCACAAAAA CGTCCTGCTCCATCTTGTCG	NM_182894
SIX3	GGGCAGAAAACATAAAAGAGGTGAC CCCAGATACAAATAAATCGTCATGC	NM_005413
SIX6	GCTGTTTATTTACTTATTTAAGAGACCGC TCTCCACACAGAACCCATCACC	NM_007374
MITF	GAGAAGAAACTGGAGCACGCC AATCTGGAGAGCAGAGACCCG	NM_198159
ATOH7	CAGCCTGGTCATCCAGTAGAACA GAGCAAATAAGTCATAAACAAAGCAAC	NM_145178
BRN3B	GCGCTCAAACCCATCCTG	NM_004575
(POU4F2)	GGCTGAATGGCAAAGTAGGC	
iSlet1	ACACCTTGGGCGGACCTGCTATG	NM_002202
	TGAAACCACACTCGGATGACTCTG	
HOXB4	CCGTCGTCTACCCCTGGATG	NM_024015
	CCGTGTCAGGTAGCGGTTGTAG	
AFP	CAAAATGCGTTTCTCGTTGCTT	NM_001134
	GTGTCCGATAATAATGTCAGCCG	
ACTB	AAGATGACCCAGATCATGTTTGAG TGAGGTAGTCAGTCAGGTCCCG	NM_001101

antibodies Nanog (Cell Signaling, Danvers, MA), Oct3/4, Pax6, Nestin, Tuj, Chx10 (all from Millipore, Temecula, CA), Sox2, ZO1, Rx, calretinin, iSlet1, synaptophysin (all from Abcam, Burlingame, CA), Otx2 (Invitrogen), Chx10 (Santa Cruz, Dallas, TX), and Rx (Santa Cruz) were used at 1:200 dilution. Pax6 (DSHB, Iowa City, IA) was used at 1:50 dilution. K_i-67 (Abcam) and Brn3b (Abcam) were used at 1:1,000 dilution. Fluorescent confocal images were acquired using a laser scanning microscope (LSM 510; Carl Zeiss, Thornwood, NY).

Flow cytometry analysis: Cells were trypsinized into single cell suspensions and then fixed in Fixation Medium Reagent A (Invitrogen; 1×10^6 cells) for 15 min, permeabilized with Permeabilization Medium Reagent B (Invitrogen), and stained with primary antibodies Chx10 (Abcam, 1:500 dilution) or Brn3b (Abcam, 1:1,000 dilution) for 20 min at room temperature, and washed once in PBS + 0.1% NaN_3 + 5% fetal bovine serum (FBS). Then the cells were incubated with fluorescein isothiocyanate (FITC)–conjugated secondary antibodies (anti-rabbit FITC, Invitrogen, 1:300) for another 20 min in the dark, washed and resuspended in PBS buffer, and analyzed with flow cytometry (FACS Aria; BD Biosciences, Franklin Lakes, NJ).

Calcium imaging: Calcium imaging of the TiPSC-derived retinal neurons was performed as described elsewhere [15,29,30]. Briefly, cells were loaded with 4 µmol/l Fluo-3/AM (Molecular Probes) and 0.02% pluronic F-127 in phenol red free medium at 37 °C for 30 min in dark. Then nonfluorescent Fluo-3/AM was de-esterified with intracellular esterases to yield fluorescent Fura-3. The Ca^{2+} concentration was reduced and replaced with EGTA buffers in low-potassium (0 Ca^{2+}) Tyrode's solutions: 129 mM NaCl, 5 mM KCl, 2 mM EGTA, 3 mM $MgCl_2$, 30 mM glucose, and 25 mM HEPES, pH 7.4. The Ca^{2+} influx was stimulated by applying stimuli such as high-potassium 2 mM Ca^{2+} Tyrode's solutions: 5 mM NaCl, 129 mM KCl, 2 mM $CaCl_2$, 1 mM $MgCl_2$, 30 mM glucose, and 25 mM HEPES, pH 7.4. The fluorescence signal was recorded with the LSM 510 confocal laser scanning system. Fluo-3 was excited at 488 nm, and emission was detected at 515–535 nm. For each condition, the fluorescence was captured every 5 s for 200 s after the Tyrode's solution was replaced.

Statistical analysis: At least three replicates were performed for each experiment. The data are presented as the mean ± standard deviation (SD). Statistical analysis of the data was performed using SPSS13.0, and significance of differences was evaluated using the unpaired Student *t* test. A p value of less than 0.05 was considered statistically significant

RESULTS

Stepwise differentiation of TiPSCs to a retinal progenitor cell fate: The established TiPSC colonies were expanded on MEF feeders, displayed typical undifferentiated hESC-like colony morphology (Figure 2A), and highly expressed pluripotency markers Nanog,Oct-4, and Sox2 but not panneural markers Pax6,Otx2, and Nestin as determined with immunofluorescence analysis (Figure 2B–D). Upon differentiation, EBs were formed by the suspension culture of TiPSCs in serum-free EB medium for 6 to 7 days with pluripotent genes *Oct3/4* and *Nanog* markedly decreased ($p<0.05$), concurrent with the onset of expression of early neuroectodermal-related genes *Pax6* and *Lhx2* ($p<0.01$) and the sustained expression of *Sox2* (Figure 2E) in the DNL induction groups and the control groups as analyzed with quantitative real-time PCR. There was no significant difference between the two groups. However, the eye field markers Rax and Chx10 were rarely detected during this period. Concurrently, immunofluorescence analysis also revealed that the majority of EBs exhibited positive immunostaining for the early neuroectodermal markers Sox2, Pax6, Otx2, and Nestin in both groups (Figure 2F–H). Thus, we conclude that TiPSC-derived EBs would preferably adopt neuroectodermal characteristics in the absence of exogenous signaling molecules, consistent with previous reports of these cells' innate neural differentiation potential [31].

To determine whether DNL treatment could promote retinal specification of TiPSCs, we next transferred EB aggregates into Matrigel-coated six-well plates in NDM supplemented with DNL and then performed an analysis of the regional markers involved in eye field specification. By day 16, a large fraction of the cells (86% of colonies, SD ± 8%, three separate experiments) adopted neural cluster-like structures with fibrous-shape cells migrating from the surroundings in the DNL groups (Figure 3A). In contrast, the colonies in the control groups exhibited a fairly flat morphology, mainly composed of undifferentiated cells with a few cells presenting random differentiation (Figure 3B). At the protein level, nearly all neural cluster-like structures (approximately 80% of the colonies) uniformly expressed retinal neural progenitor markers Pax6, Chx10, and Rx after DNL treatment, as determined with immunocytochemistry (Figure 3C–E). Otx2+/ZO1+ rosette-like clusters were also observed in the DNL cultures (Figure 3F). ZO-1 is a marker for tight junctions and is expressed in the lumen of neural rosettes, a feature associated with progenitor populations [9,32]. Thus, the expression patterns of neural cluster-like structures were reminiscent of the optic vesicle stage of retinal development, confirming their multipotent RPC identities.

By day 21, quantitative real-time PCR analysis also revealed that DNL treatment substantially increased the expression levels of eye field transcription factors (EFTFs) such as Rax, Chx10 (the retina and diencephalon), Six3, and Six6 (rostral diencephalon; 5.3- to 6.0-fold upregulation, $p<0.05$), and correspondingly largely suppressed spinal cord-associated transcription factor HoxB4 ($p<0.05$) and the endoderm marker of alpha-fetoprotein (AFP; $p<0.01$) when compared with the control group (Figure 3G). The data also showed the expression levels of *Pax6* and *Lhx2* were further upregulated in both groups after attachment, approximately 2.2 and 2.4 times upregulation after the addition of DNL, respectively. These results indicated the process of obtaining an early eye field fate was enhanced through the addition of DKK1, Noggin, and Lefty A.

Moreover, the expression of the RGC markers, including *Atoh7* and *Brn3b*, was upregulated by day 21, although the relative expression increase was modest in the study. Approximately, 1.8 and 2.4 times upregulation of each was observed in the DNL induction groups when compared with the control groups, concurrent with the comparable 2.2 times upregulation of the *Pax6* levels after DNL treatment. This finding is consistent with previous reports that Pax6 acting as an Atoh7 upstream gene could directly activate *Atoh7* [33] but, in the present investigation, not sufficient to upregulate *Atoh7* and *Brn3b* to a certain extent to give rise to a RGC phenotype during this period. These results indicated that TiPSCs could differentiate into the earliest stages of retinogenesis in a stepwise manner, and DNL treatment could substantially promote this retinal specification process.

Purification and expansion of RPCs: Phase contrast images of representative cluster-like structures displayed tightly packed colony morphology (Figure 3A), while randomly differentiated colonies displayed undifferentiated or flat epithelium-like morphology (Figure 3B). The central portions of the neural cluster structures were selectively lifted from periphery flat cells or non-neuroepithelial cells under the microscope and replated on Matrigel-coated six-well plates to allow single-cell RPC outgrowth, yielding neural clusters with highly enriched Chx10+ cells (from 63.70% to 85.87% of Chx10+ cells with fluorescence-activated cell sorting (FACS) analysis, Figure 4A). After 5–10 days,

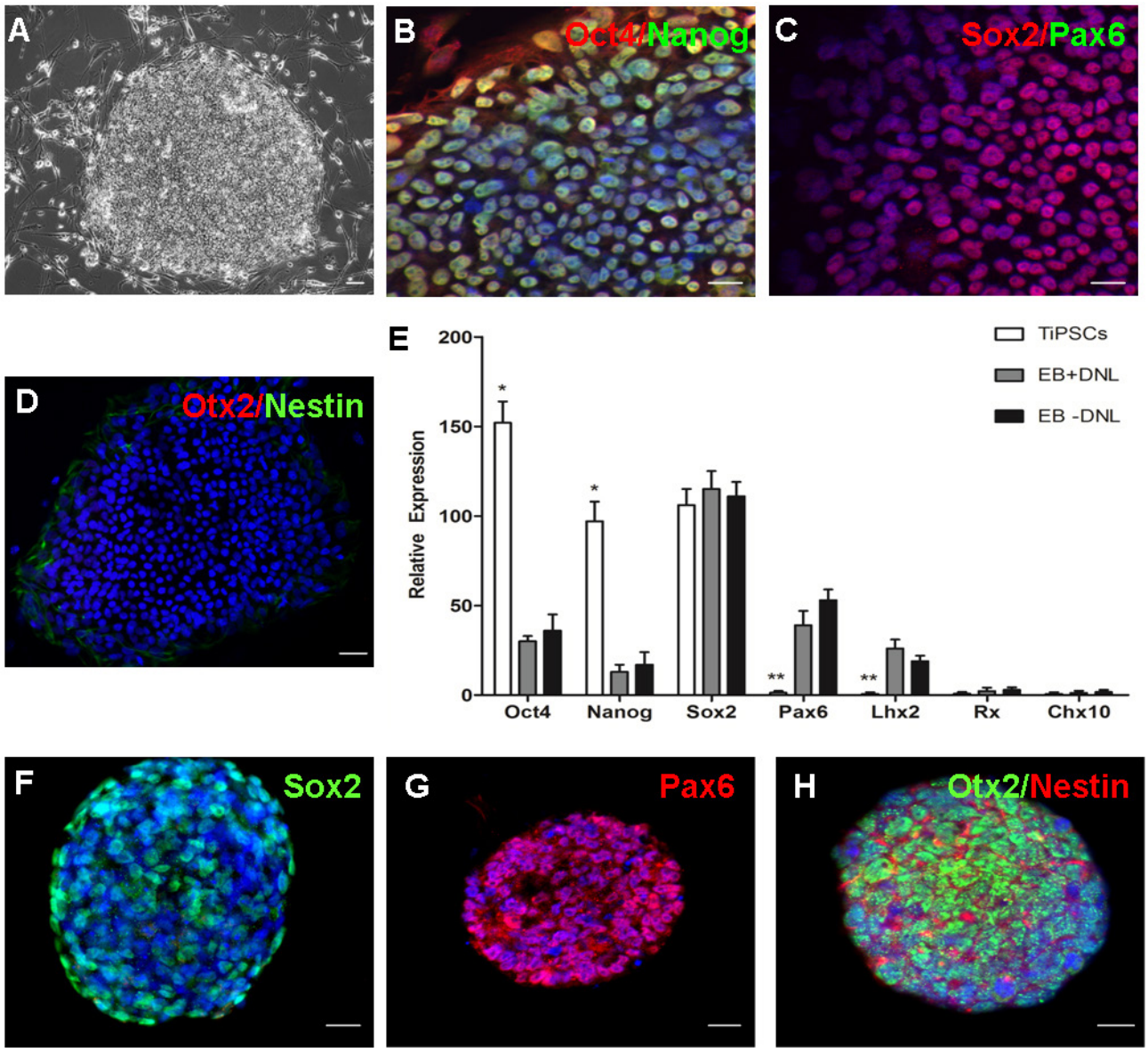

Figure 2. Primitive neuroectodermal specification of human TiPSCs through EB formation. **A**: Phase contrast images of an established Tenon's-derived induced pluripotent stem cell (TiPSC) line at passage P 33, displaying typical undifferentiated human embryonic stem cell (hESC)-like colony morphology. Scale bar = 100 µm. **B**–**D**: Confocal immunofluorescent images of undifferentiated TiPSC clones, stained positive for pluripotency associated markers Oct-4, Nanog, and Sox2 but negative for panneural markers Pax6, Otx2, and Nestin. Nuclei were stained with 4',6-diamidino-2-phenylindole (DAPI). Scale bars = 50 µm. **E**: Quantitative real-time PCR analysis confirmed pluripotent genes *Oct3/4* and *Nanog* markedly decreased after 6 days of suspension culture (* $p<0.05$), concurrent with the equivalent upregulation of early neuroectodermal-associated genes *Pax6* and *Lhx2* in two groups (** $p<0.01$). Transcript levels were normalized to ACTB levels. The graph shows the mean ± standard deviation (SD; n = 3). **F**–**H**: Confocal immunofluorescent images of embryonic bodies (EBs) stained with early neuroectodermal markers Sox2, Pax6, Otx2, and Nestin. Scale bars = 50 µm.

migratory single cell-RPCs formed a monolayer to fill the gaps between the clusters (Figure 4B) and highly expressed RPC-related marker Pax6 as determined with confocal immunofluorescence analysis (Figure 4C–D). Then these purified neural cluster structures with a highly enriched population of RPCs were dissociated into single cells with TrypLE and then further maintained and expanded in RPC medium+1% Matrigel. The single-cell RPCs thus generated displayed typical neural stem cell morphology (Figure 4E) and highly expressed RPC-related markers Chx10, Rx, and ki67 as determined by confocal immunofluorescence analysis (Figure 4F–G). Concurrent with a previous study,

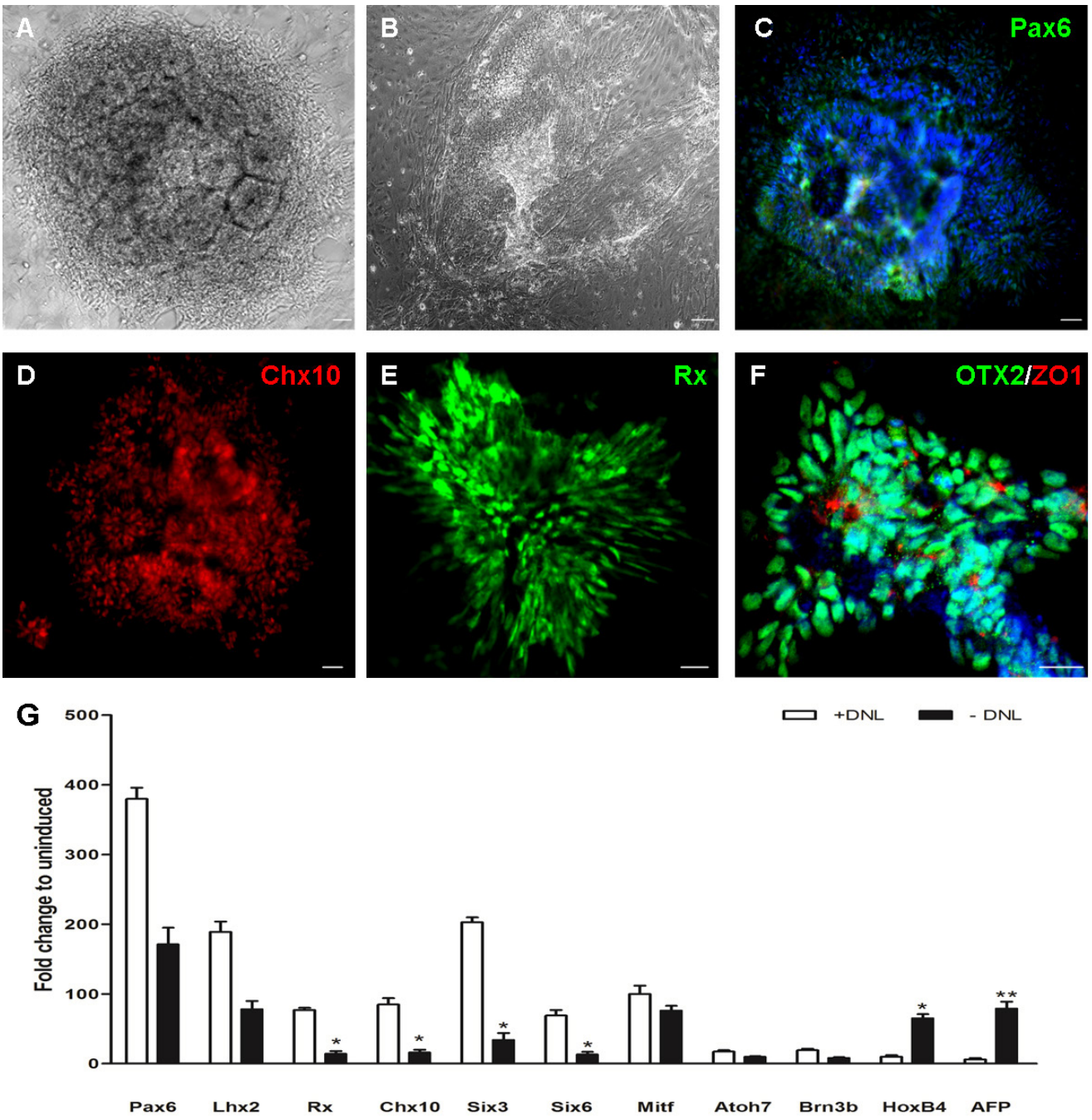

Figure 3. Directed derivation of RPCs with the addition of DKK1, Noggin, and Lefty A. **A**–**B**: Phase contrast images of representative Tenon's-derived induced pluripotent stem cell (TiPSC)-derived neuroepithelial colonies (**A**, displaying tightly packed colony morphology) and randomly differentiated colonies (**B**, displaying flat non-neural morphology) after 10 days of culture on Matrigel. Scale bar = 100 µm. **C**–**F**: Confocal images of neuroepithelial colonies stained with early eye field markers Pax6, Chx10, Rx, Otx2, and ZO1. Scale bars = 100 µm. **G**: Quantitative real-time PCR analysis showed *Pax6* and *Lhx2* were further upregulated in both groups after attachment for another 10 days, whereas eye field-specific regional genes *Rax*, *Chx10*, *Six3*, and *Six6* are upregulated substantially in the DNL group when compared with the control group (* $p<0.05$); correspondingly, *HOXB4* (the hindbrain and spinal cord) and *AFP* (an endoderm marker) are largely suppressed in the DNL group (* $p<0.05$, ** $p<0.01$). + = the DNL group, - = the control group. Transcript levels were normalized to ACTB levels. The graph above shows the mean ± standard deviation (SD; n = 3).

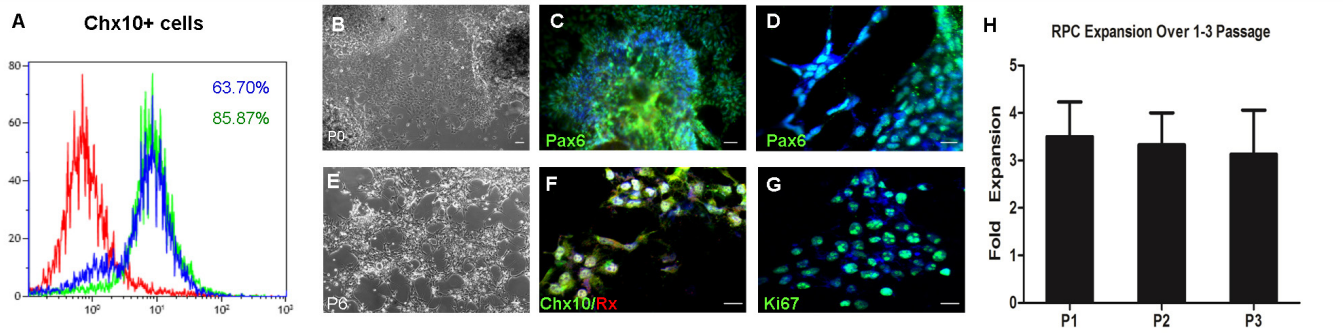

Figure 4. Purification and expansion of RPCs. **A**: Fluorescence-activated cell sorting (FACS) analysis showed Chx10-positive proliferating retinal progenitor cells were further enriched after manual selection, approximately from 63.70% to 85.87%. Blue line: before selection, green line: after selection. **B**: Phase contrast images of P0 retinal progenitor cells (RPCs). Single-cell RPCs have emerged from replated neuroepithelial clusters and formed a monolayer after 5–6 days. Scale bar = 50 µm. **C**–**D**: Confocal images of P0 RPCs stained with early eye field markers Pax6 (**C**, low magnification; **D**, high magnification). Scale bar = 50 µm. **E**: Phase contrast images of established RPC line at passage P6. Neuroepithelial clusters were further dissociated for the single-cell RPC sub-culture. Scale bar = 50 µm. **F**–**G**: Confocal images of dispersed RPCs stained with eye field markers Chx10, Rx, and Ki67. Scale bars = 50 µm. **H**: Dispersed RPCs were efficiently propagated three- to fourfold once a week on average in the RPC medium. The graph above shows the mean ± standard deviation (SD; n = 3).

Ki67+ proliferative RPCs predominated, reminiscent of the neuroblastic layer within the developing human retina. In the presence of mitogen, the RPCs were efficiently propagated through at least ten passages (three- to fourfold once a week on average; Figure 4H).

Acquisition of RGC phenotypes by Atoh7 overexpression: We then asked whether the induced RPCs could further be specified to differentiate into the RGC phenotype. Our previous study demonstrated the essential role of *Atoh7* as the RGC-specific regulator for RGC specification in a mouse iPS line [27]. Therefore, in this study, we sought to determine whether forced expression of *Atoh7* in human TiPSC-derived RPCs could also activate RGC-specified gene expression and eventually give rise to a RGC phenotype.

Twenty-four hours after infection, about 80% of the RPC cells were successfully transfected under this transfection condition as monitored with GFP-expressing vectors (data not shown). The qRT-PCR analysis further demonstrated *Atoh7* gene expression markedly increased 72 h after transfection ($p<0.005$; Figure 5A). As the cultures continued, cells initiated the expression of *Atoh7* downstream genes *Brn3b* and *iSlet1*, approximately 6.6 and 9.0 times upregulation, respectively ($p<0.05$; Figure 5B), indicative of the onset of RGC genesis. Unlike previous miPSC lines, supplementing Notch inhibition of DAPT did not appear to increase the expression of RGC-related transcription factors in the present investigation (data not shown). As the genes increased over time, a subset displayed RGC-like neuron morphology with elongated, straight synapse-like structures (Figure 5C). The RGC-like cells were stained positive for Brn3b, Tuj, iSlet1, calretinin, and synaptophysin (Figure 5D–F). Moreover, confocal calcium imaging analysis further confirmed that the Fluo-3 AM loaded RGC-like cells established appropriate Ca^{2+} activity in response to EGTA and high-potassium Tyrode's solution (Figure 5G). Under these conditions, we observed with FACS analysis that approximately 23.14% of the total cells were immunopositive for the RGC-specific marker Brn3b (Figure 5H). These data indicated that DNL-induced retinal progenitors are competent to differentiate into a RGC phenotype in response to *Atoh7* overexpression.

DISCUSSION

The generation of RGCs from iPS is of considerable interest as they can be used as cell replacement therapy for treating glaucoma, a neurodegenerative disease of the eye caused by the degeneration of RGCs. In this study, we mimicked the retinal developmental process to design a three-step method to achieve targeted RGC differentiation, relying on the administration of instructive signals (DKK1+Noggin+Lefty A) and a lineage–specific regulator (*Atoh7*). The results indicate that TiPSCs, serving as a renewable source of RPCs by responding to simulated environment signaling, can be further programmed to assume the RGC phenotype through *ATOH7* overexpression, which, for the first time, demonstrated the validity of using *Atoh7* for RGC induction in the context of human iPSC lines.

When recapitulating in vivo retinal differentiation, TiPSCs pass through an anterior neuroectoderm-like stage first by suspension culture in the serum-free medium, and then a subset attains an RPC identity in the subsequent

Matrigel-coated culture with the addition of DKK1, Noggin, and Lefty A, a combination of developmental stimuli factors that had been used in previous protocols to mimic the micro-environmental signals of retinogenesis [3]. Cells were identified as early as day 16 and then selectively isolated under the microscope and maintained in the presence of mitogen for multiple passages. With further overexpression of *Atoh7*, a subset gradually assumed the RGC phenotype, and about 23% of the *Brn3b*-positive RGC-like cells were obtained finally. These cells, alongside reliable differentiation, purity, and expansion of RPCs, combined with additional genetic manipulation is sufficient to promote RGC specification from iPS, setting the stage for the future successful application of cell replacement therapy for RGC regeneration.

During the earliest histogenesis stages, we observed the comparable elevation of primitive ectodermal markers in EBs differentiated under minimal culture conditions, consistent with the EBs' reported neural differentiation propensity [31]. However, this limited competence is heavily dependent on cell line–specific endogenous signaling [34,35],

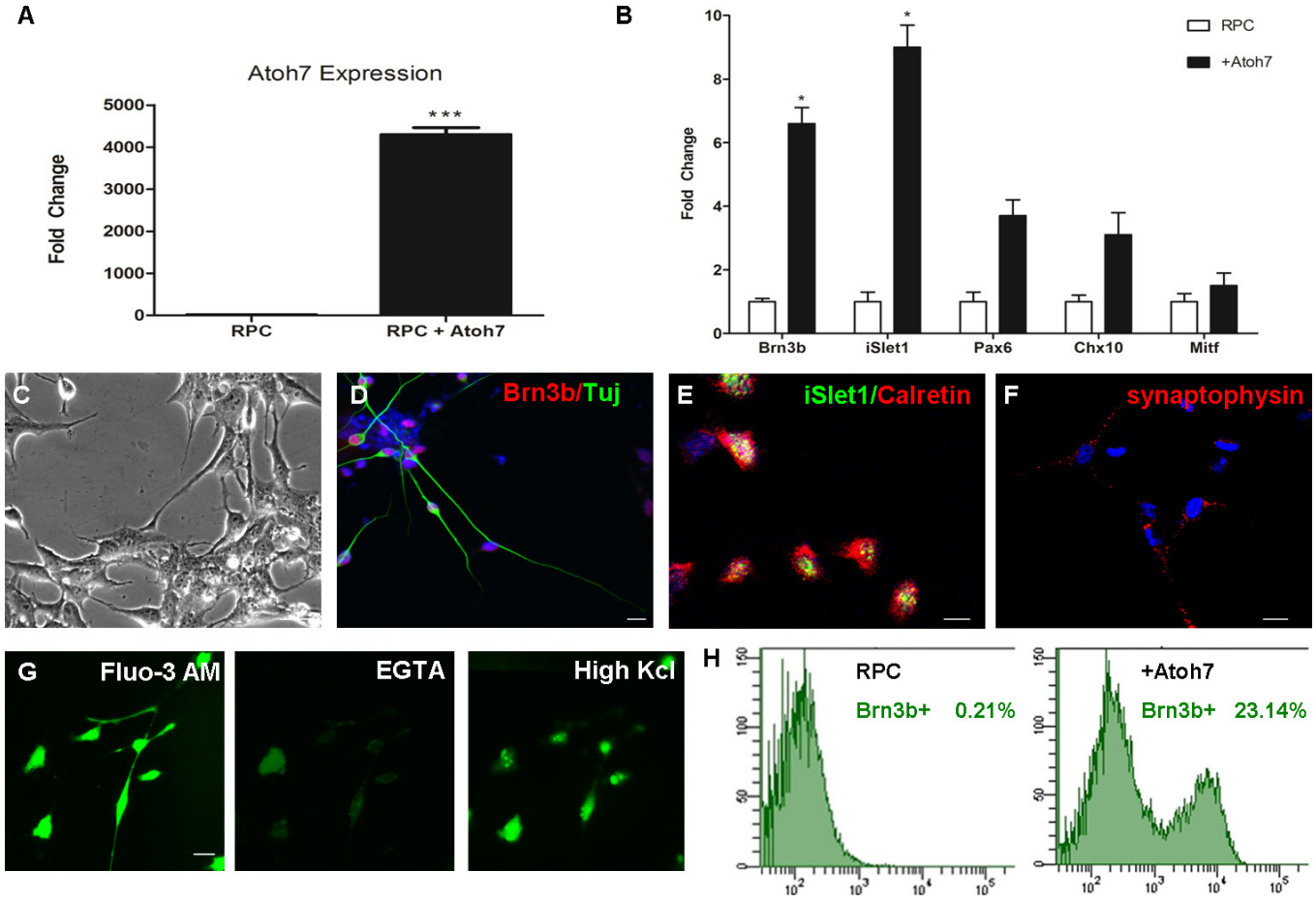

Figure 5. Acquisition of RGC phenotypes with *Atoh7* overexpression. **A**: Quantitative real-time PCR analysis showed *Atoh7* gene expression is demonstrably upregulated with transfection of the Atoh7 vector (*** $p<0.005$). Transcript levels were normalized to ACTB levels. The graph shows the mean ± standard deviation (SD; n = 3). **B**: Quantitative real-time PCR analysis confirmed *Atoh7* overexpression activated RGC-related genes *Brn3b* and *iSlet1* (* $p<0.05$). Transcript levels were normalized to ACTB levels. The graph shows the mean ± standard deviation (SD; n = 3). **C**: Phase contrast images of transfected cell displaying RGC-like neuron morphology. Scale bar = 50 µm. **D**–**F**: Confocal immunofluorescent images of RGC-like cells, stained positive for Brn3b, Tuj, iSlet1, calretinin, and synaptophysin. Scale bars = 50 µm. **G:** Ca^{2+} image of RGC-like cells loaded with Fluo-3 AM showed the Ca^{2+} influx was reduced by EGTA and stimulated with high-potassium Tyrode's solution. Left panel: a confocal image of the representative cell loaded with Fluo-3 AM Middle panel: after the application of EGTA Tyrode's solution, Ca^{2+} concentration was reduced with diminished fluorescence intensity, captured at 25 s. Right panel: after the application of high-potassium Tyrode's solution, Ca^{2+} influx was stimulated with increased fluorescence intensity, captured at 35 s. Scale bars = 50 µm. **H**: Fluorescence-activated cell sorting (FACS) analysis showed approximately 23% of derived retinal neural cells were positive for Brn3b.

which is far from enough to achieve highly homogeneous neural differentiation for clinical use. Particularly, the EBs' intrinsic propensity was correlated with early endogenous expression of DKK1, Noggin, Lefty A, and so on [5,8,9,36], which are known to influence anterior neurogenesis. We have since used this information to optimize culture conditions to direct the differentiation path. In doing so, acquisition of the neuroretinal phenotype was substantially enhanced with EFTF expression increased by 5.3- to 6.0-fold during the Matrigel-coated culture. Additionally, cytokine stimulation further homogenized the culture to a purer RPC yield by correspondingly blocking non-retinogenic differentiation programs. Results have shown this modified protocol efficiently pushed retinal differentiation in a selective induction manner.

After a 2-week treatment, we observed the emergence of neural cluster-like structures, which present an original optic vesicle (OV) phenotype revealed by coexpression of EFTFs [5,8,9,37]. Thus, their readily discernible appearances and corresponding OV identities imply it is possible to monitor neural differentiation merely with direct light microscopic inspection. In this study, tightly packed neural clusters were identified as early as day 16, and then the central portions were mechanically manipulated into generating neural aggregates consisting of a nearly uniform population of proliferating Chx10+ RPCs. Thus, regarding neural clusters as an indicator of early eye field formation could allow the identification, selection, and enrichment of desired cell types in the absence of an antibody or reporter, enhancing their clinical advantages.

The high proliferation capability of RPCs is appealing in establishing cell therapy strategies because it allows rapid acquisition of banks of RPCs to sustain clinical use. In this regard, high-quality RPC cultures with a low proportion of spontaneous differentiation are crucial. However, long-term floating cultures of neurosphere-like structures would eventually allow multipotent RPCs to develop into more mature cell types and lost their progenitor identities, which is probably evoked by cell–cell interactions within aggregates [5,6]. Thus, we split neural cluster-like structures into single cells to reduce cellular interactions and modified the culture medium with 1% Matrigel added to promote cell adhesion. Under this condition, the RPCs were easily passaged and amplified while retaining their phenotype for at least ten passages. After serial passaging, we obtained a large-scale well-characterized RPC pool for downstream differentiation.

Once RPCs exit the cell cycle, they commit to a more restricted lineage-competent state. During vertebrate retinogenesis, RGCs are the first cell type to be specified, and the fate determination process involves a hierarchical gene regulatory network [20]. *Atoh7* is a member of the *bHLH* family and its spatiotemporal expression pattern is consistent with RGC genesis. Previous studies have confirmed *Atoh7*'s critical regulatory role in RGC genesis [18,25]. In this report, we transfected human TiPSC-derived RPCs with the *Atoh7* expression vector in an attempt to promote RGC specification. Consistent with previous findings [27], a subset of transfected cells acquired neuron morphology and expressed genes and proteins characteristic of RGC precursors, including *Brn3b* and *iSlet1*. Additionally, the established cells displayed the appropriate physiologic properties of cellular calcium activities in vitro. Thus, the overall developmental patterns of the recorded cells resembled that of the authentic RGCs, indicative of their committed RGC identities. Finally, approximately 23% of Brn3b-positive RGC-like cells were obtained in this DKK1+Noggin+Lefty A/*Atoh7*-based RGC in vitro differentiation system.

A critical gap in the investigation, however, was the disproportionate relation between transfection efficacy and induction efficacy (approximately 80% versus 23%), suggesting not all progenitor cells that express *Atoh7* eventually advance to a committed RGC fate. As an essential upstream regulator, *ATOH7* plays a key role in the establishment of RGC competence and subsequent control of RGC differentiation [19]. It has been proposed that, during RGC genesis, the initial wave of *Atoh7* confers postmitotic precursors with RGC competence by providing a favorable intrinsic environment for activation of the RGC differentiation cascade [38]. However, *Atoh7* alone is not sufficient to specify the RGC lineage; presumably, other downstream factors are needed to enable RGC-competent precursors to accomplish the final conversion [39]. Adding to the complexity of this system, recently it has been proposed that a small subset of RGCs form from *Neurod1*-expressing precursors in a parallel pathway independent of *ATOH7* [40,41]. The pathway to RGC commitment remains an intricate and incompletely understood process, and more work needs to be done to elucidate how these genes function in the transcriptional network circuitry. Unlike previous mouse iPSC (miPSC) lines [27], supplementing Notch inhibition of DAPT does not appear to increase the expression of RGC-related transcription factors in this investigation, suggesting that, not surprisingly, there may be species-specific differences between mouse and human iPSC lines in terms of RGC induction, or probably the transient exposure to high *Atoh7* could overcome the negative regulation of the Notch signaling pathway.

Precise, efficient, and controlled directed differentiation of hPSCs is an important goal of regenerative medicine.

Based on previous investigations, we devised a targeted and multidimensional RGC induction strategy for TiPSCs. Upon retinal differentiation, the TiPSCs initially yielded a highly enriched population of early eye field cells with DNL treatment. Moreover, using manual isolation techniques to selectively recover neural aggregates could allow for neuronal cell enrichment in the absence of an antibody or reporter. These TiPSC-derived RPC intermediaries, which are routinely >85% Chx10+ with FACS analysis, may be further expanded and frozen before differentiation allowing for a convenient downstream experiment. Last, by introducing the master transcription factor ATOH7, about 23% of the treated cells acquired RGC-like cell identities. In conclusion, our synergistic induction strategies combined with DNL treatment and *Atoh7* overexpression can efficiently direct the stage-specific differentiation of human TiPSC toward RGC lineage, which should aid in the future therapeutic application of patient-tailored cellular material to replace injured RGCs that occur in glaucoma.

ACKNOWLEDGMENTS

This study was supported by National Natural Science Foundation of China Grants 81371007, 81430009, Science and Technology Planning Projects of Guangdong Province Grant 2014B020225001, Science and Technology Program of Guangzhou Grant 15570001, and Fundamental Research Funds of the State Key Laboratory of Ophthalmology Grant 2012IP02.

REFERENCES

1. Wright LS, Phillips MJ, Pinilla I, Hei D, Gamm DM. Induced pluripotent stem cells as custom therapeutics for retinal repair: progress and rationale. Exp Eye Res 2014; 123:161-72. [PMID: 24534198].
2. Cyranoski D. Stem cells cruise to clinic. Nature 2013; 494:413-[PMID: 23446394].
3. Borooah S, Phillips MJ, Bilican B, Wright AF, Wilmut I, Chandran S, Gamm D, Dhillon B. Using human induced pluripotent stem cells to treat retinal disease. Prog Retin Eye Res 2013; 37:163-81. [PMID: 24104210].
4. Sluch VM, Zack DJ. Stem cells, retinal ganglion cells and glaucoma. Dev Ophthalmol 2014; 53:111-21. [PMID: 24732765].
5. Meyer JS, Howden SE, Wallace KA, Verhoeven AD, Wright LS, Capowski EE, Pinilla I, Martin JM, Tian S, Stewart R, Pattnaik B, Thomson J, Gamm DM. Optic vesicle-like structures derived from human pluripotent stem cells facilitate a customized approach to retinal disease treatment. Stem Cells 2011; 29:1206-18. [PMID: 21678528].
6. Phillips MJ, Wallace KA, Dickerson SJ, Miller MJ, Verhoeven AD, Martin JM, Wright LS, Shen W, Capowski EE, Percin EF, Perez ET, Zhong XF, Canto-Soler MV, Gamm DM. Blood-Derived Human iPS Cells Generate Optic Vesicle-Like Structures with the Capacity to Form Retinal Laminae and Develop Synapses. Invest Ophthalmol Vis Sci 2012; 53:2007-19. [PMID: 22410558].
7. Zhong X, Gutierrez C, Xue T, Hampton C, Vergara MN, Cao LH, Peters A, Park TS, Zambidis ET, Meyer JS, Gamm DM, Yau KW, Canto-Soler M. Generation of three-dimensional retinal tissue with functional photoreceptors from human iPSCs. Nat Commun 2014; 5:4047-[PMID: 24915161].
8. Mellough CB, Sernagor E, Moreno-Gimeno I, Steel DH, Lako M. Efficient stage-specific differentiation of human pluripotent stem cells toward retinal photoreceptor cells. Stem Cells 2012; 30:673-86. [PMID: 22267304].
9. Meyer JS, Shearer RL, Capowski EE, Wright LS, Wallace KA, McMillan EL, Zhang SC, Gamm DM. Modeling early retinal development with human embryonic and induced pluripotent stem cells. Proc Natl Acad Sci USA 2009; 106:16698-703. [PMID: 19706890].
10. Takahashi K, Tanabe K, Ohnuki M, Narita M, Ichisaka T, Tomoda K, Yamanaka S. Induction of pluripotent stem cells from adult human fibroblasts by defined factors. Cell 2007; 131:861-72. [PMID: 18035408].
11. Yu J, Vodyanik MA, Smuga-Otto K, Antosiewicz-Bourget J, Frane JL, Tian S, Nie J, Jonsdottir GA, Ruotti V, Stewart R, Slukvin II, Thomson JA. Induced pluripotent stem cell lines derived from human somatic cells. Science 2007; 318:1917-20. [PMID: 18029452].
12. Zhou L, Wang W, Liu Y, Fernandez de Castro J, Ezashi T, Telugu BP, Roberts RM, Kaplan HJ, Dean DC. Differentiation of induced pluripotent stem cells of swine into rod photoreceptors and their integration into the retina. Stem Cells 2011; 29:972-80. [PMID: 21491544].
13. Watanabe K, Kamiya D, Nishiyama A, Katayama T, Nozaki S, Kawasaki H, Watanabe Y, Mizuseki K, Sasai Y. Directed differentiation of telencephalic precursors from embryonic stem cells. Nat Neurosci 2005; 8:288-96. [PMID: 15696161].
14. Cavodeassi F, Carreira-Barbosa F, Young RM, Concha ML, Allende ML, Houart C, Tada M, Wilson SW. Early stages of zebrafish eye formation require the coordinated activity of Wnt11, Fz5, and the Wnt/beta-catenin pathway. Neuron 2005; 47:43-56. [PMID: 15996547].
15. Lamba DA, Karl MO, Ware CB, Reh TA. Efficient generation of retinal progenitor cells from human embryonic stem cells. Proc Natl Acad Sci USA 2006; 103:12769-74. [PMID: 16908856].
16. Hirami Y, Osakada F, Takahashi K, Okita K, Yamanaka S, Ikeda H, Yoshimura N, Takahashi M. Generation of retinal cells from mouse and human induced pluripotent stem cells. Neurosci Lett 2009; 458:126-31. [PMID: 19379795].
17. . Gruss TMaP. Generating neuronal diversity in the retina.pdf. Trends Neurosci 2002; 25:32-8. [PMID: 11801336].
18. Matter-Sadzinski L, Puzianowska-Kuznicka M, Hernandez J, Ballivet M, Matter JM. A bHLH transcriptional network

regulating the specification of retinal ganglion cells. Development 2005; 132:3907-21. [PMID: 16079155].

19. Zhiyong Yang KD, Pan L, Deng M, Gan L. Math5 determines the competence state of retinal ganglion cell progenitors. Dev Biol 2003; 264:240-54. [PMID: 14623245].

20. Mu X, Klein WH. A gene regulatory hierarchy for retinal ganglion cell specification and differentiation. Semin Cell Dev Biol 2004; 15:115-23. [PMID: 15036214].

21. Nadean L, Brown TG. Math5 is required for retinal ganglion cell and optic nerve formation.pdf. Development 2001; 128:2497-508. [PMID: 11493566].

22. Wang SWKB, Ding K, Wang H, Sun D, Johnson RL, Klein WH, Gan L. Requirement for math5 in the development of retinal ganglion cells. Genes Dev 2001; 15:24-9. [PMID: 11156601].

23. Kay JNF-BK, Roeser T, Staub W, Baier H. Retinal ganglion cell genesis requires lakritz, a zebrafish atonal homolog. Neuron 2001; 30:725-36. [PMID: 11430806].

24. Liu W, Xiang M. The Ath5 proneural genes function upstream of Brn3POU domain transcription factor genes to promote retinal ganglion cell development. Proc Natl Acad Sci USA 2001; 98:1649-54. [PMID: 11172005].

25. Nadean L, Brown SK, Monica L. Vetter,Tom Glaser. Math5 encodes a murine basic helix-loophelix transcription factor. Development 1998; 125:4821-33. [PMID: 9806930].

26. Kanekar S, Dorsky R, Harris WA, Jan LY, Jan YN, Vetter ML. Xath5 participates in a network of bHLH genes in the developing Xenopus retina. Neuron 1997; 19:981-94. [PMID: 9390513].

27. Chen M, Chen Q, Sun XR, Shen W, Liu B, Zhong X, Leng Y, Li C, Zhang W, Chai F, Huang B, Gao QY, Xiang AP, Zhuo YH, Ge J. Generation of retinal ganglion-like cells from reprogrammed mouse fibroblasts. Invest Ophthalmol Vis Sci 2010; 51:5970-8. [PMID: 20484577].

28. Deng F, Hu HL, Chen MF, Sun XR, Liu XH, Dong ZZ, Liu Y, Xi L, Zhuang J, Ge J. Generation of Induced Pluripotent Stem Cells from Human Tenon's capsule fibroblasts. Mol Vis 2012; 18:2871-81. [PMID: 23233789].

29. Suzuki N, Shimizu J, Takai K, Arimitsu N, Ueda Y, Takada E, Hirotsu C, Suzuki T, Fujiwara N, Tadokoro M. Establishment of retinal progenitor cell clones by transfection with Pax6 gene of mouse induced pluripotent stem (iPS) cells. Neurosci Lett 2012; 509:116-20. [PMID: 22230895].

30. Kwan HY, Shen B, Ma X, Kwok YC, Huang Y, Man YB, Yu S, Yao X. TRPC1 associates with BK(Ca) channel to form a signal complex in vascular smooth muscle cells. Circ Res 2009; 104:670-8. [PMID: 19168436].

31. Pankratz MT, Li XJ, Lavaute TM, Lyons EA, Chen X, Zhang SC. Directed neural differentiation of human embryonic stem cells via an obligated primitive anterior stage. Stem Cells 2007; 25:1511-20. [PMID: 17332508].

32. Elkabetz Y, Panagiotakos G, Al Shamy G, Socci ND, Tabar V, Studer L. Human ES cell-derived neural rosettes reveal a functionally distinct early neural stem cell stage. Genes Dev 2008; 22:152-65. [PMID: 18198334].

33. Riesenberg AN, Le TT, Willardsen MI, Blackburn DC, Vetter ML, Brown NL. Pax6 regulation of Math5 during mouse retinal neurogenesis. Genesis 2009; 47:175-87. [PMID: 19208436].

34. Kim DS, Lee JS, Leem JW, Huh YJ, Kim JY, Kim HS, Park IH, Daley GQ, Hwang DY, Kim DW. Robust enhancement of neural differentiation from human ES and iPS cells regardless of their innate difference in differentiation propensity. Stem Cell Rev 2010; 6:270-81. [PMID: 20376579].

35. Grabel L. Prospects for pluripotent stem cell therapies: into the clinic and back to the bench. J Cell Biochem 2012; 113:381-7. [PMID: 21928325].

36. Ying QL, Stavridis M, Griffiths D, Li M, Smith A. Conversion of embryonic stem cells into neuroectodermal precursors in adherent monoculture. Nat Biotechnol 2003; 21:183-6. [PMID: 12524553].

37. Zuber ME, Gestri G, Viczian AS, Barsacchi G, Harris WA. Specification of the vertebrate eye by a network of eye field transcription factors. Development 2003; 130:5155-67. [PMID: 12944429].

38. Chiodini F, Matter-Sadzinski L, Rodrigues T, Skowronska-Krawczyk D, Brodier L, Schaad O, Bauer C, Ballivet M, Matter JM. A positive feedback loop between ATOH7 and a Notch effector regulates cell-cycle progression and neurogenesis in the retina. Cell Reports 2013; 3:796-807. [PMID: 23434507].

39. Mu X, Fu X, Sun H, Beremand PD, Thomas TL, Klein WH. A gene network downstream of transcription factor Math5 regulates retinal progenitor cell competence and ganglion cell fate. Dev Biol 2005; 280:467-81. [PMID: 15882586].

40. Mao CA, Wang SW, Pan P, Klein WH. Rewiring the retinal ganglion cell gene regulatory network: Neurod1 promotes retinal ganglion cell fate in the absence of Math5. Development 2008; 135:3379-88. [PMID: 18787067].

41. Kiyama T, Mao CA, Cho JH, Fu X, Pan P, Mu X, Klein WH. Overlapping spatiotemporal patterns of regulatory gene expression are required for neuronal progenitors to specify retinal ganglion cell fate. Vision Res 2011; 51:251-9. [PMID: 20951721].

Articles are provided courtesy of Emory University and the Zhongshan Ophthalmic Center, Sun Yat-sen University, P.R. China. The print version of this article was created on 28 May 2016. This reflects all typographical corrections and errata to the article through that date. Details of any changes may be found in the online version of the article.